Vibronic Coupling through the In-Phase, C=C Stretching Mode Plays a Major Role in the $2A_g^-$ to $1A_g^-$ Internal Conversion of *all-trans-β*-Carotene

Hiroyoshi Nagae

Kobe City University of Foreign Studies, Gakuen-Higashimachi, Nishi-ku, Kobe 651-2187, Japan

Michitaka Kuki

Department of Applied Chemistry, Kobe City College of Technology, Gakuen-Higashimachi, Nishi-ku, Kobe 651-2194, Japan

Jian-Ping Zhang, Tokutake Sashima, Yumiko Mukai, and Yasushi Koyama*

Faculty of Science, Kwansei Gakuin University, Uegahara, Nishinomiya 662-8501, Japan

Received: July 19, 1999; In Final Form: October 19, 1999

The major role of vibronic coupling through the in-phase, C=C stretching (ν_1) mode in the $2A_g^-$ to $1A_g^-$ internal conversion of *all-trans-β*-carotene has been shown by the use of isotopic effects on the rate of internal conversion and on the strength of vibronic coupling as follows: (1) The rates of internal conversion for *all-trans-β*-carotene having natural abundance isotope composition [NA], along with ^{2}H-labeled [^{2}H], ^{13}C-labeled [^{13}C], and ^{2}H,^{13}C-doubly labeled [^{2}H,^{13}C] *all-trans-β*-carotenes, were determined, by subpicosecond time-resolved absorption spectroscopy, to be in the ratio [NA]/[^{2}H]/[^{13}C]/[^{2}H,^{13}C] = 1:0.92:0.70:0.64. (2) The strength of vibronic coupling was estimated for each isotope species by using the frequency difference between the $2A_g^-$ and $1A_g^-$ states, which was determined, by picosecond Raman spectroscopy, to be in the ratio, [NA]/[^{2}H]/[^{13}C]/[^{2}H,^{13}C] = 1:1.21:0.89:1.07. On the other hand, a theory was presented to show that the nonadiabatic vibronic-coupling constant that determines the rate of internal conversion is proportional to the adiabatic vibronic-coupling constant that determines the frequency difference. The application of the observed relative strength of vibronic coupling to the Englman−Jortner equation, for a single mode ν_1, predicted the relative rates of internal conversion to be 1:0.80:0.72:0.60, which are in good agreement with those observed above. (3) A theory showing that the adiabatic vibronic-coupling constant is proportional to the product of the transition bond-order matrix and the *L* matrix was also presented. In a polyene model, the relative rates of internal conversion were predicted to be 1:0.94:0.68:0.64, which are in excellent agreement with the above observed values.

Introduction

Carotenoids in the all-trans configuration are selectively bound to the antenna complexes in purple photosynthetic bacteria and in other photosynthetic organisms[1] and play an important role in light harvesting.[2−4] It is generally accepted that there are two channels of singlet-energy transfer, one from the $1B_u^+$ state of carotenoid to the Q_x state of bacteriochlorophyll (BChl) and the other from the $2A_g^-$ state of carotenoid to the Q_y state of BChl. In the case of the LH2 complex of *Rhodobacter sphaeroides* 2.4.1, containing *all-trans*-spheroidene and BChl *a* (see Figure 1), the former energy-transfer reaction shortens the $1B_u^+$ lifetime of carotenoid from 150 fs (in solution) to 80 fs,[5] and the latter energy transfer shortens the $2A_g^-$ lifetime of carotenoid from 10 to 2 ps (Zhang et al., unpublished results). These values lead to a time constant of 170 fs and an efficiency of 47% for the former singlet-energy transfer and to a time constant of 2.5 ps and an efficiency of 42% for the latter singlet-energy transfer. The results indicate that the energy-transfer reactions compete with those fast internal-conversion processes within the carotenoid that are considered to be most important in dissipating the excess energy.

Concerning the $1B_u^+$ to $2A_g^-$ internal conversion, which is predicted to be symmetry-forbidden within the framework of the Pariser−Parr−Pople (PPP) approximation, the $1B_u^-$ state, which has been newly found in this particular carotenoid, exists between those states and is supposed to play a crucial role in this internal conversion (see ref 6 for details). On the other hand, concerning the $2A_g^-$ to $1A_g^-$ internal conversion of this carotenoid, the extremely high frequency of the in-phase, C=C stretching mode (hereafter, abbreviated as the ν_1 mode) in the $2A_g^-$ state[7] and a large Franck−Condon factor shown in the fluorescence from the $2A_g^-$ state[8] suggest the presence of strong vibronic coupling between the $2A_g^-$ and $1A_g^-$ states mediated by the ν_1 mode.

The major role of the ν_1 mode in the $2A_g^-$ to $1A_g^-$ vibronic coupling and internal conversion has been suggested in the case of *all-trans-β*-carotene for the first time. The presence of vibronic coupling between the $2A_g^-$ and $1A_g^-$ states of carotenoid was first evidenced by transient-Raman spectroscopy,[9,10] and the role of this vibronic coupling in dissipating the excess energy by enhancing the internal conversion was suggested.[9] The small effects of deuteration and of lowering

* To whom correspondence should be addressed. Fax: +81-798-51-0914. Phone: +81-798-54-6389. E-mail: ykoyama@kwansei.ac.jp.

10.1021/jp9924833 CCC: $19.00
Published on Web 01/22/2000

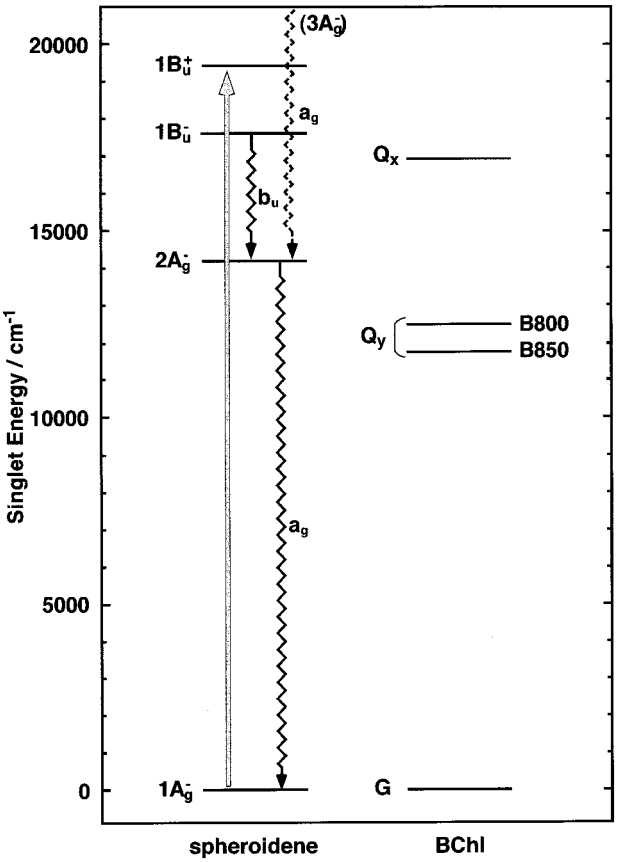

Figure 1. Energy diagram for *all-trans*-spheroidene and BChl *a* in the LH2 antenna complex from *R. sphaeroides* 2.4.1. The $1B_u^+$ level of spheroidene and the Q_x and Q_y levels of BChl *a* were determined by electronic-absorption spectroscopy of the complex, and the optically forbidden $1B_u^-$ and $2A_g^-$ levels of spheroidene were determined in the crystalline state by measurements of resonance-Raman excitation-profile.[6,34] Indicated are excitation upon absorption of photon as well as the internal-conversion processes facilitated by vibronic couplings through different normal modes.

temperature on the $2A_g^-$ lifetime of *all-trans*-β-carotene in 3-methyl-pentane solution excluded the possible involvement of the C−H stretching and bending modes, as well as that of the low-frequency skeletal modes in this particular internal-conversion process.[11] Calculated changes in bond order upon excitation from the $1A_g^-$ to the $2A_g^-$ state also suggested a large Franck−Condon factor of the ν_1 mode to enhance this process.[11]

In the present investigation, we have addressed the question, "Why is the $2A_g^-$ lifetime of this carotenoid (on the order of 10^{-11} s) so short?" We have attempted, by the use of isotopic effects, to establish the role of vibronic coupling through the ν_1 mode in the $2A_g^-$ to $1A_g^-$ internal conversion of *all-trans*-β-carotene (hereafter, simply denoted as β-carotene). First, we purified β-carotene of natural abundance isotope composition [NA] as well as totally ^{2}H-labeled [^{2}H], ^{13}C- labeled [^{13}C], and ^{2}H,^{13}C-doubly labeled [^{2}H,^{13}C] β-carotenes that had been extracted from the cells of algae grown in isotope-substituted media. Second, we determined the $2A_g^-$ to $1A_g^-$ internal conversion rates of those β-carotenes by subpicosecond time-resolved absorption spectroscopy. Third, we determined, by picosecond transient-Raman spectroscopy, the ν_1 frequencies of those β-carotenes in both the $2A_g^-$ and the $1A_g^-$ states. Fourth, we developed a theory showing that the nonadiabatic vibronic-coupling constant that determines the rate of internal conversion is proportional to the adiabatic vibronic-coupling constant that determines the frequency shifts of the ν_1 mode through the vibronic coupling. Next, we calculated the relative rates of the internal conversion of isotopic β-carotenes (in reference to that of the [NA] species, which was normalized to unity) by the use of the Englman−Jortner equation.[12] This was accomplished by regarding (1) the difference in the ν_1 frequency between the two electronic states as a measure of the vibronic coupling strength, and (2) the $1A_g^-$-state ν_1 frequency as that of the accepting mode. The agreement between the observed and the calculated relative rates of internal conversion provided evidence for the notion that the ν_1 mode plays a major role in the $2A_g^-$ to $1A_g^-$ vibronic coupling and internal conversion.

Finally, we developed another theory showing that the adiabatic vibronic-coupling constant is proportional to a product of the transition bond-order matrix and the *L* matrix. We calculated the transition bond-order matrix between the $2A_g^-$ and $1A_g^-$ states for a model polyene (docosaundecaene), by the PPP method and the *L* matrixes of the isotope-labeled species by normal-coordinate analysis for the model polyene. The excellent agreement of the calculated relative rates of internal conversion with those observed has established the notion that the ν_1 mode plays a dominant role in the $2A_g^-$ to $1A_g^-$ internal conversion and that it shortens the $2A_g^-$ lifetime.

Methods

Theory of Internal Conversion and Vibronic Coupling. In the adiabatic approximation or the Born−Oppenheimer (BO) approximation, the state of the system is described by a product of wave functions,

$$\Psi_{nv} = \psi_n \Theta_{nv} \tag{1}$$

where ψ_n is the wave function for the electrons of the system (the nuclei are considered to be fixed at their instantaneous positions) and Θ_{nv} is the wavefuncion of intramolecular nuclear vibrations; *n* and *v* specify the electronic and vibrational states. ψ_n and Θ_{nv} are the solutions of the following coupled Schrödinger equations,

$$H_e(Q)\psi_n(Q) = E_n(Q)\psi_n(Q) \tag{2}$$

$$[T(Q) + E_n(Q)]\Theta_{nv}(Q) = W_{nv}\Theta_{nv}(Q) \tag{3}$$

where $Q = \{Q_j\}$ represents a set of nuclear normal coordinates. Equation 2 contains *Q* parametrically.

In the BO approximation, the perturbation that causes the internal conversion process between a pair of electronic states is the kinetic energy of the nuclei; the kinetic energy and the perturbation[13] are given by

$$T(Q) = {}^1/_2 \sum_j \left(-i\hbar \frac{\partial}{\partial Q_j}\right)^2 \tag{4}$$

$$H'\Psi_{nv} = -\hbar^2 \sum_j \frac{\partial \psi_n \partial \Theta_{nv}}{\partial Q_j\, \partial Q_j} - {}^1/_2 \hbar^2 \sum_j \frac{\partial^2 \psi_n}{\partial Q_j^2} \Theta_{nv} \tag{5}$$

The second terms of eq 5 can be neglected when compared to the first term for the region in which the BO approximation can normally be expected to hold.[14] Then, under the condition that the energy gap between the initial and the final electronic states is large, compared to the vibrational energies (the statistical limit), the rate of internal conversion from the *n*th to

the mth electronic state can be expressed as[12]

$$k = \frac{2\pi}{\hbar} C^2 \sum_u \sum_v B_v |\langle \Theta_{nv} | \Theta_{mu} \rangle|^2 \delta(\Delta E + E_v - E_u) \quad (6)$$

with

$$C^2 = \sum_j \left| \hbar\omega_j \left\langle \psi_n \left| \frac{\partial}{\partial q_j} \right| \psi_m \right\rangle_{q=q^0} \right|^2 \quad (7)$$

where B_v is the Boltzmann factor, ΔE is the difference in electronic energy between the initial and final states $[E_n(q^0) - E_m(q^0)]$, E_v and E_u are the vibrational energies of the initial and the final states, ω_j is the adiabatic angular frequency of the jth normal mode, and q_j is the dimensionless normal coordinate

$$q_j = \sqrt{\frac{\omega_j}{\hbar}} Q_j \quad (8)$$

and q^0 represents the equilibrium nuclear geometry of the initial state. Here, C is called the nonadiabatic vibronic-coupling constant. A normal mode whose amount of the C^2 term is substantial is referred to as "the promoting mode". A normal mode whose shift of the potential minimum from the initial to the final state is large is called "the accepting mode". For a case in which one of the accepting modes is predominant, the rate of internal conversion can be approximately written as[12]

$$k = \frac{2\pi}{\hbar} C^2 \frac{1}{\sqrt{2\pi(\Delta E)\hbar\omega}} \exp(-{}^1/_2\Delta^2) \exp\left(-\frac{\gamma(\Delta E)}{\hbar\omega}\right) \quad (9)$$

with

$$\gamma = \ln\frac{2(\Delta E)}{\Delta^2 \hbar\omega} - 1 \quad (10)$$

where ω and Δ are the adiabatic angular frequency and the shift of the accepting mode along the dimensionless normal coordinate, respectively. This equation is derived under the assumption that the difference in the vibrational frequencies between the electronic states can be disregarded.

The first-order nonadiabatic vibronic-coupling matrix element can be given, within the framework of the PPP theory dealing with the π electrons as separate from the σ electrons, as follows:

$$\left\langle \psi_n(q) \left| \frac{\partial \psi_m(q)}{\partial q_i} \right\rangle_{q=q^0} = \left\langle \bar{\psi}_n(q) \left| \frac{\partial \bar{\psi}_m(q)}{\partial q_i} \right\rangle_{q=q^0} + \frac{\left\langle \bar{\psi}_n(q) \left| \sum_{r\neq s,\sigma} \left(\frac{\partial \beta_{rs}}{\partial q_i} - {}^1/_2 P_{rs} \frac{\partial \gamma_{rs}}{\partial q_i} \right) a_{r\sigma}^\dagger a_{s\sigma} \right| \bar{\psi}_m(q) \right\rangle_{q=q^0}}{\bar{E}_m(q_0) - \bar{E}_n(q_0)} \quad (11)$$

where the bar (—) signifies that a floating atomic basis set or a diabatic set is being used, β_{rs} and γ_{rs} are the resonance integral and the effective electron−electron repulsion integral between the rth and sth π orbitals, respectively, P_{rs} is the bond order between the rth and sth atoms in the ground state, and $a_{r\sigma}^\dagger$ and $a_{r\sigma}$ are the fermion creation and annihilation operators which respectively create and annihilate an electron with spin σ in the rth mutually orthogonal atomic π orbital. The numerator of the second term on the right-hand side is called the adiabatic vibronic-coupling matrix element ($V_j^{(n,m)}$), and it changes the diabatic frequency of normal mode (vide infra). It can be shown that the first term on the right-hand side becomes negligible in a planar conjugated molecule (the details will be published elsewhere; Nagae, H. to be published). Thus,

$$\left\langle \psi_n \left| \frac{\partial}{\partial q_j} \right| \psi_m \right\rangle_{q=q^0} = \frac{V_j^{(m,n)}}{(E_m(q^0) - E_n(q^0))} \quad (12)$$

For a case in which the vibronic coupling by the jth mode is strong only between the nth and mth electronic states, the adiabatic frequencies can be expressed as[15]

$$\omega_j^{(n)} \equiv \Omega_j + \frac{|V_j^{(m,n)}|^2}{\hbar[E_n(q^0) - E_m(q^0)]} \quad (13)$$

$$\omega_j^{(m)} \equiv \Omega_j - \frac{|V_j^{(m,n)}|^2}{\hbar[E_n(q^0) - E_m(q^0)]} \quad (14)$$

where Ω_j and ω_j are called the diabatic and the adiabatic frequencies, respectively. It follows that, for each vibrational mode, the adiabatic frequency of the lower state decreases, whereas that of the upper state increases by the same amount. Therefore, the difference in the adiabatic frequency between the two electronic states is directly proportional to the square of the adiabatic vibronic coupling constant,

$$\omega_j^{(n)} - \omega_j^{(m)} = \frac{2|V_j^{(n,m)}|^2}{\hbar[E_n(q^0) - E_m(q^0)]} \quad (15)$$

Thus, the nonadiabatic vibronic-coupling constant that determines the rate of internal conversion (C) can be regarded as being proportional to the adiabatic vibronic-coupling constant (V) that determines the frequency difference of the normal mode mediating the vibronic coupling between the relevant states.

The adiabatic vibronic-coupling constant, $V_j^{(n,m)}$, can be expressed in terms of the transition bond-order matrix, $P_{rs}^{(n,m)}$, and the L matrix,

$$V_j^{(n,m)} = 2\sqrt{\frac{\hbar}{\omega_j^{(m)}}} \sum_{r>s} \left(\frac{\partial \beta_{rs}}{\partial R_{rs}} - {}^1/_2 P_{rs} \frac{\partial \gamma_{rs}}{\partial R_{rs}} \right)_{q=q^0} P_{rs}^{(n,m)} L_{rs,j} \quad (16)$$

where

$$P_{rs}^{(n,m)} = {}^1/_2 (\langle \psi_n | \sum_\sigma (a_{r\sigma}^\dagger a_{s\sigma} + a_{s\sigma}^\dagger a_{r\sigma} | \psi_m \rangle)_{q=q^0} \quad (17)$$

and

$$L_{rs,j} = \left(\frac{\partial R_{rs}}{\partial Q_j} \right)_{q=q^0} \quad (18)$$

Here, R_{rs} is the distance between the rth and sth atoms, and Q_j is a normal coordinate.

Calculation of the Transition Bond-Order Matrixes and the *L* Matrixes. The transition bond-order matrixes, which were previously called "bond transition-density matrixes"[16] and then renamed, according to Donnath,[17] were calculated for transition from either the $1A_g^-$ or the $2A_g^-$ state to other low-lying singlet states for a model polyene (docosaundecaene) by the PPP method, as described previously.[6,18] The C═C and C−C bond lengths were assumed to be 1.35 and 1.46 Å, respectively, and the C═C−C bond angle was assumed to be 120°.

The *L* matrixes were calculated for a polyene model and for a β-carotene model having the methyl groups attached to the conjugated chain, the structures of which were assumed to be as follows: In the polyene model, (1) the C═C, C−C, and C−H bond lengths were assumed to be 1.35, 1.46, and 1.10 Å, respectively, (2) the C═C−C and C═C−H bond angles were fixed to 120°, and (3) the conjugated chain was assumed to be in a planar all-trans configuration. In the β-carotene model, (1) the β-ionone ring was simplified by replacing the first and fourth skeletal carbon atoms by a pair of "dummy" 15 mass units, and (2) the rotational angle around the C6−C7 bond was fixed to be 60°. (3) A planar, all-trans configuration was assumed for the rest of the conjugated chain, and (4) the bond lengths and the bond angles were taken from the results of X-ray crystallography.[19] The normal-coordinate analysis was performed by Wilson's GF-matrix method using a Urey−Bradley−Shimanouchi (UBS) force field; in some cases, non-UBS cross terms were also introduced. The programs GCCC, BGLZ, and LSMB, which had been originally written in Professor Takehiko Shimanouchi's laboratory,[20] were run on a Micro VAX 2900 computer at the Faculty of Science and a PC/AT compatible personal computer.

Preparation of Isotopic β-Carotenes. [NA] β-Carotene was purchased from Wako Pure Chemical Industries (Osaka) and recrystallized twice from benzene. [^{13}C] β-Carotene was extracted, with acetone, from the cells of *Chlamydomonas reinhardtii* C-9 grown in the tris-acetate-phosphate medium;[21] $^{13}CH_3{}^{13}COONa$ was used as a carbon source.[22] [^{2}H] β-Carotene was extracted from the cells of *Chlorella* sp. WT-1 grown by the use of the ^2H_2O-substituted Myers' C medium in Chlorella Industries Inc (Tokyo). The acetone extract of [^{2}H,^{13}C] β-carotene was a gift from Chlorella Industries Inc. A mixture of 1,4-dioxane and water (1:1) was added to each acetone extract of the isotope-labeled photosynthetic pigments to crystallize chlorophyll *a*,[23] and the supernatant after centrifugation was used for further purification of the carotenoid.

The recrystallized [NA] β-carotene and the crude [^{2}H], [^{13}C], and [^{2}H,^{13}C] β-carotenes were purified by repeating a series of column chromatography[8] using (a) silica gel (Merck, silica gel 60) as adsorbate and 5% 2-propanol in *n*-hexane as eluent and (b) alumina (Merck, aluminum oxide 90, activity II−III) as adsorbate and 1−3% diethyl ether in *n*-hexane as eluent. The all-trans isomer was collected from each β-carotene component thus purified by HPLC using calcium hydroxide (Nacalai Tesque, GR, lot M6N0577) as adsorbate and 0.5−1% acetone in *n*-hexane as eluent.[24,25] Each purified all-trans isomer exhibited a single peak in HPLC when detected at 450 nm. The enrichment factor of [^{2}H] β-carotene was determined to be 98% by HPLC ([^{2}H] elutes more slowly than [NA]). The enrichment factor of [^{13}C] β-carotene was determined to be 95%, whereas the enrichment factors of ^{2}H and ^{13}C in [^{2}H,^{13}C] β-carotene were determined to be 70% and 95%, respectively, by means of NMR spectroscopy.

Subpicosecond Time-Resolved Absorption Spectroscopy. A set of time-resolved absorption spectra of each β-carotene in flowing *n*-hexane solution (8×10^{-5} M, 12−15 mL) was recorded as described previously[26] except for the following modifications: (1) A regenerative amplifier (Spectra Physics, Spitfire) that was seeded by a mode-locked Ti:sapphire laser (Spectra Physics, Tsunami) generated the 800 nm pulses (120 fs, 1 kHz and 1 mJ/pulse); the laser beam was divided into two components by using a 10% thin-film beam splitter. The major component was sent to an optical parametric amplifier (Spectra Physics, OPA-800) which generated the 476 nm pulses (130 fs, 1 kHz, 4 μJ); the power for pumping the sample was reduced down to 0.2−0.3 μJ/pulse. The minor component was focused into a water cell to generate a white continuum. The fwhm of the cross correlation trace between the pump and the probe pulses was determined to be 250 fs by the use of optical Kerr-effect signal. (2) The photon density applied to the sample solution was 1.5×10^{14} photons·cm^{-2}. The number of absorbed photons and the number of molecules in the beam were estimated to be 8.6×10^{10} and 4.7×10^{12}, respectively.

Picosecond Transient-Raman Spectroscopy. The Raman spectra of each β-carotene in both the $1A_g^-$ (ground) and the $2A_g^-$ (S_1) states were recorded for a 2×10^{-4} M tetrahydrofuran solution (500 μL) sealed in an ampule, which was used as a rotating Raman cell. A pair of Raman spectra were recorded with high (25 mW) and low (2.5 mW) laser power by the use of the SH pulses (527 nm, 50 ps, and 1 kHz) from a combination of a mode-locked Nd:YLF laser (Quantronix 4216) and a Nd:YLF regenerative amplifier (Quantronix 4417). A 90° Raman scattering was recorded on a Raman spectrometer (JASCO TRS-300) equipped with an image-intensified, diode-array detector (Princeton Instruments IRY-700). The data-accumulation time was 198 and 792 s for the high-power and the low-power measurements, respectively. The low-power spectrum was regarded as the $1^1A_g^-$-state spectrum, whereas a difference spectrum of the high-power spectrum minus the low-power spectrum was regarded as the $2A_g^-$-state spectrum.

Results and Discussion

Isotopic Effects on the Rate of the $2A_g^-$ to $1A_g^-$ Internal Conversion Determined by Subpicosecond Time-Resolved Absorption Spectroscopy. Figure 2 shows the subpicosecond, time-resolved absorption spectra of (a) [NA], (b) [^{2}H], (c) [^{13}C], and (d) [^{2}H,^{13}C] β-carotenes in *n*-hexane solution. At −0.2 ps, two sharp negative peaks appear; we will call the stronger peak, at 488 nm (20 500 cm^{-1}), "peak a", and the weaker peak, at 527 nm (19 000 cm^{-1}), "peak b". They can be interpreted as follows: (i) The energy of peak a is lower than that of the $1B_u^+(0) \leftarrow 1A_g^-(0)$ absorption at 478 nm (20 900 cm^{-1}) by 400 cm^{-1}, and therefore, it can be definitely assigned to the $1B_u^+(0) \rightarrow 1A_g^-(0)$ fluorescence (stimulated emission). This Stokes shift roughly agrees with that of *all-trans*-β-carotene at 170 K (300 cm^{-1}), which was determined by stationary-state electronic absorption and fluorescence spectroscopy.[27] (ii) The $1B_u^+(1) \leftarrow 1A_g^-(0)$ absorption appears at 449 nm (22 300 cm^{-1}), and the spacing between the $1B_u^+(1) \leftarrow 1A_g^-(0)$ and the $1B_u^+(0) \leftarrow 1A_g^-(0)$ absorptive transitions, 1400 cm^{-1}, roughly agrees with the spacing between peak a and peak b, 1500 cm^{-1}. Therefore, peak b can be assigned to the $1B_u^+(0) \rightarrow 1A_g^-(0)$ fluorescence (stimulated emission). The relative intensity of fluorescent peak b/peak a is much lower than that of the $1B_u^+(1) \leftarrow 1A_g^-(0)/1B_u^+(0) \leftarrow 1A_g^-(0)$ absorptive peaks, an observation which can be explained in terms of the overlap of the $S_n \leftarrow 2A_g^-$ transient absorption.

The slightly structured, transient-absorption profile appearing in the 500−600 nm region, which increases at longer delay times at the expense of the bleaching of the $1B_u^+ \leftarrow 1A_g^-$ absorption, can be definitely assigned to the $S_n \leftarrow 2A_g^-$ absorption. This transient absorption can be used to determine the $2A_g^-$ lifetime, that is, the rate of the $2A_g^-$ to $1A_g^-$ internal conversion. Comparison of the spectra of isotopic β-carotenes at 20 ps suggests longer $2A_g^-$ lifetimes for [^{13}C] and [^{2}H,^{13}C] β-carotenes.

Figure 3 compares the time profiles at 554 nm (the maximum of the transient absorption) for (a) [NA], (b) [^{2}H], (c) [^{13}C],

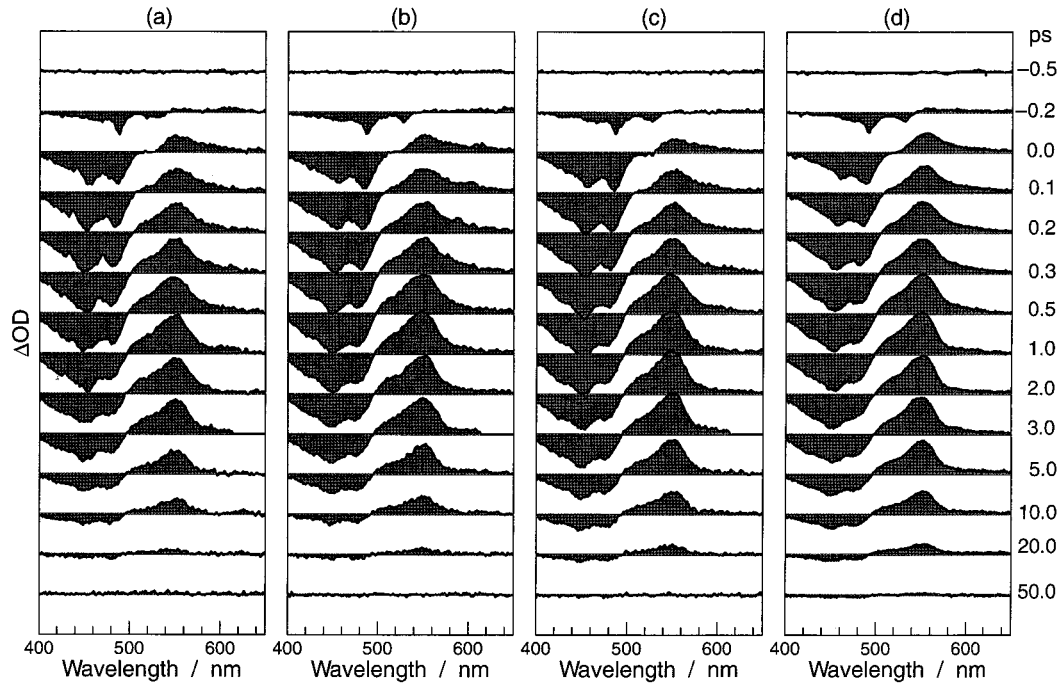

Figure 2. Time-resolved, electronic-absorption spectra of (a) [NA], (b) [^{2}H], (c) [^{13}C], and (d) [^{2}H,^{13}C] *all-trans*-β-carotenes in *n*-hexane solution after excitation at 476 nm.

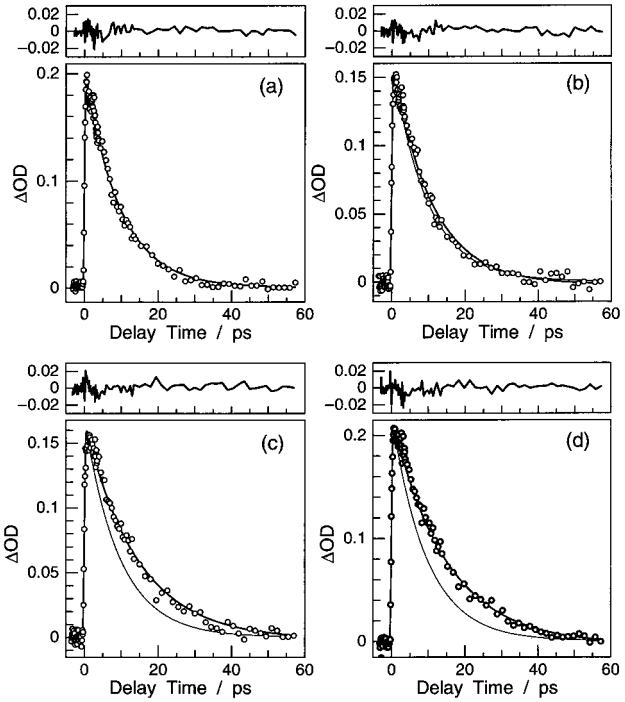

Figure 3. Time profiles for (a) [NA], (b) [^{2}H], (c) [^{13}C], and (d) [^{2}H,^{13}C] *all-trans*-β-carotenes probed at 554 nm. Each strong line indicates fitting to the observed data points, and the residual is shown on the top of each panel. Thin solid lines indicate the fitting curve for [NA] *all-trans*-β-carotene for comparison.

and (d) [^{2}H,^{13}C] β-carotenes. Each strong solid line indicates a single-exponential fitting curve to the data points; the residual after fitting is shown on the top of each panel. In panels b−d, the fitting curve for [NA] β-carotene is shown as a weak solid line for comparison. It is obvious that the ^{2}H substitution affects little, but the ^{13}C substitution substantially lengthens the $2A_g^-$ lifetime, a fact which suggests that the skeletal stretching or bending modes (rather than the C−H stretching or bending mode) play a predominant role in the $2A_g^-$ to $1A_g^-$ internal-conversion process.

TABLE 1: The $2A_g^-$ Lifetimes (Rates of the $2A_g^-$ to1 A_g^- Internal Conversion) and Frequencies of the In-Phase, C═C Stretching (ν_1) Mode in the $2A_g^-$ and $1A_g^-$ States for [NA], [^{2}H], [^{13}C], and [^{2}H,^{13}C] *all-trans*-β-Carotenes

	[NA]	[^{2}H]	[^{13}C]	[^{2}H,^{13}C]
τ^a	9.92	10.73	14.27	15.58
k^b	10.1	9.32	7.01	6.42
(ratio)	1.00	0.92	0.70	0.64
$\nu_1(2A_g^-)^c$	1781	1772	1720	1713
$\nu_1(1A_g^-)^c$	1522	1458	1489	1435
$\Delta\nu^c$	259	314	231	278
(ratio)	1.00	1.21	0.89	1.07

[a] The $2A_g^-$ lifetime in 10^{-12} s. [b] The rate of the $2A_g^-$ to $1A_g^-$ internal conversion in 10^{10} s^{-1}. [c] The ν_1 frequency in the $2A_g^-$ and $1A_g^-$ states and their difference all in cm^{-1}.

Table 1 lists the $2A_g^-$ lifetimes and the rates of the $2A_g^-$ to $1A_g^-$ internal conversion for [NA], [^{2}H], [^{13}C], and [^{2}H,^{13}C] β-carotenes. The ratio of the rate of internal conversion is now determined to be 1:0.92:0.70:0.64.

Isotopic Effects on the Strength of Vibronic Coupling between the $2A_g^-$ and $1A_g^-$ States As Determined by Transient-Raman Spectroscopy. Figure 4 shows the $1A_g^-$ (ground)-state Raman spectra of (a) [NA], (b) [^{2}H], (c) [^{13}C], and (d) [^{2}H,^{13}C] β-carotenes. The assignment of each Raman line was given on the basis of normal-coordinate analysis using a set of force constants that had been determined for [NA] and deuterated species, including 11-*d*, 11,11′-d_2, 14-*d*, 14,14′-d_2, 15-*d*, and 15,15′-d_2 β-carotenes (Mukai et al., unpublished results).

(a) [NA] β-Carotene. The weak profiles at 1590 and 1577 cm^{-1} can be assigned to the terminal C_7═C_8 and C_9═C_{10} stretchings, and the strong peak at 1522 cm^{-1} can be assigned to the in-phase C_{11}═C_{12} and C_{13}═C_{14} stretchings in the central part. The weak peaks at 1448 and 1396 cm^{-1} can be assigned to the methyl degenerate and symmetric deformations, respectively. The weak profiles at 1356, 1280, 1269 and 1256 cm^{-1}

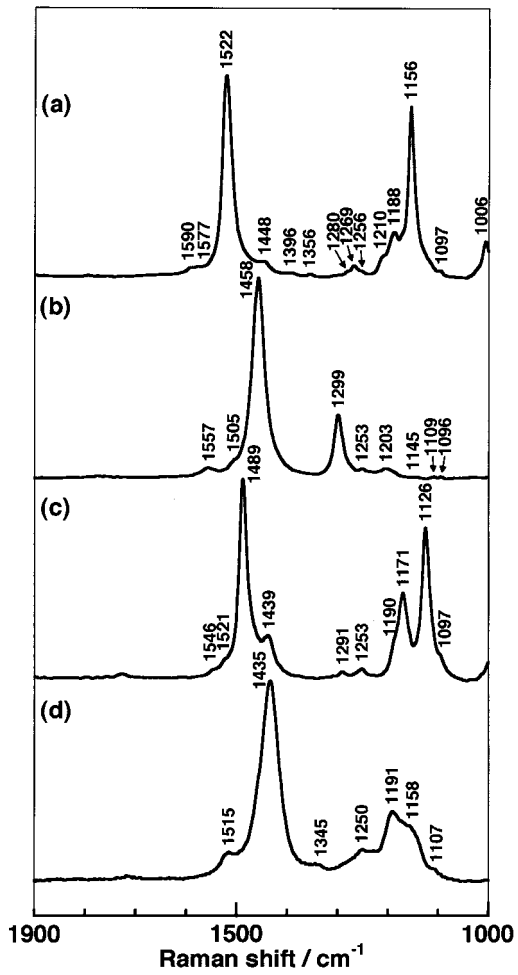

Figure 4. $1A_g^-$ (ground)-state Raman spectra of (a) [NA], (b) [^{2}H], (c) [^{13}C], and (d) [^{2}H,^{13}C] *all-trans*-β-carotenes in tetrahydrofuran (THF) solution (probed at 527 nm). Each Raman spectrum that was recorded with low power is regarded as a Raman spectrum in the $1A_g^-$ state.

can be assigned to the C−H in-plane bendings. The stronger peaks at 1210 and 1188 cm^{-1} can be assigned to the $C_{12}-C_{13}$ and C_8-C_9 stretchings, and the strong 1156 cm^{-1} peak can be assigned to the $C_{14}-C_{15}$ and $C_{10}-C_{11}$ in-phase stretchings in the central part. The 1006 cm^{-1} peak can be assigned to the methyl in-plane rockings.

(b) [^{2}H] β-Carotene. The 1557 and 1505 cm^{-1} weak profiles can be assigned to the peripheral $C_7=C_8$ and $C_9=C_{10}$ stretchings (hereafter, we will simply call them "peripheral C=C stretchings"), and the strong Raman line at 1458 cm^{-1} can be assigned to the $C_{13}=C_{14}$ and $C_{11}=C_{12}$ in-phase stretchings in the central part ("central C=C stretchings"). The medium peak at 1299 cm^{-1} can be assigned to a mixture of the $C_{12}-C_{13}$, C_8-C_9, and C_6-C_7 stretchings. The weak profiles at 1253 and 1203 cm^{-1} include the $C_{14}-C_{15}$ stretching. The weak peaks in the 1145−1096 cm^{-1} region can be ascribed to the methyl (CD_3) symmetric deformations. Because the C−H bendings of [NA] β-carotene in the 1300−1200 cm^{-1} region shift down to <1000 cm^{-1} upon deuteration and become decoupled from the C=C and C−C stretchings, the C=C stretchings shift downward, and the C−C stretchings shift upward. Thus, the predominant C=C and C−C stretching bands become closer.

(c) [^{13}C] β-Carotene. Weak shoulders at 1546 and 1521 cm^{-1} can be assigned to the peripheral C=C stretchings, and the strong peak at 1489 cm^{-1} can be definitely assigned to the central C=C stretchings. The 1439 medium Raman line is ascribable to methyl degenerate deformations. The 1291 and 1253 cm^{-1} Raman lines can be assigned to the C−H in-plane bendings, and the 1171 and 1126 cm^{-1} Raman lines can be assigned to the C_8-C_9 and $C_{14}-C_{15}$ + $C_{10}-C_{11}$ stretchings, respectively. The entire spectral pattern of [NA] β-carotene is shifted to the lower frequencies upon ^{13}C substitution, with some modification of the spectral pattern.

(d) [^{2}H,^{13}C] β-Carotene. A weak profile at 1515 cm^{-1} can be assigned to a peripheral C=C stretching, and the strong 1435 cm^{-1} line can be assigned to the in-phase, central C=C stretchings. The 1250, 1191, and 1158 cm^{-1} Raman lines can be assigned to the peripheral and the central C−C stretchings mixed together (the 1345 cm^{-1} Raman line is left unassigned). The 1107 cm^{-1} line can be assigned to the methyl symmetric deformations downshifted by deuteration. Here, the C−H bending vibrations shift down to <1000 cm^{-1} upon deuteration, as in the case of [^{2}H] β-carotene, and the entire spectral pattern of [^{2}H] β-carotene is shifted to the lower frequencies by ^{13}C substitution, with some modification of the spectral pattern.

Thus, the assignment of the strongest Raman line to the ν_1 mode, that is, the in-phase, C=C stretchings in the central part of the conjugated chain, has been established for each species of isotope. The high-Raman intensity supports this assignment to a central, in-phase mode. That the frequency of the ν_1 mode existed as low as <1530 cm^{-1} in [NA] could not be substantiated by normal-coordinate calculation without introducing either the effect of the vibronic coupling with the $2A_g^-$ (S_1) state or the off-diagonal carbon−carbon stretching force constants (these two can be proven to be equivalent, see the Appendix). Without the off-diagonal stretching force constants, the ν_1 frequency turns out to be >1650 cm^{-1} (vide infra). The normal coordinate analysis showed that the ν_2 mode, that is, the in-phase, C−C stretchings in the central part, is not always well-defined because of the coupling with the C−H in-plane bendings and the methyl in-plane deformations.

Figure 5 shows the $2A_g^-$ (S_1)-state Raman spectra of (a) [NA], (b) [^{2}H], (c) [^{13}C], and (d) [^{2}H,^{13}C] β-carotenes. A unique feature in each spectrum is the presence of a Raman line having an extraordinarily high frequency (>1700 cm^{-1}). This Raman line has been assigned to the in-phase, C=C stretching (ν_1) mode which is pushed to the higher frequencies by vibronic coupling with the $1A_g^-$ state.[9,10] The substantially low ν_1 frequency in the $1A_g^-$ state mentioned above also supports this interpretation. The ν_1 mode mediating vibronic coupling between the $2A_g^-$ and the $1A_g^-$ states pushes the ν_1 frequency upward in the upper $2A_g^-$ state and downward in the lower $1A_g^-$ state (see eqs 13 and 14 in the theoretical subsection of the Methods section). Thus, differences in the ν_1 frequency between the $1A_g^-$ and $2A_g^-$ states can be used as a measure of the strength of the adiabatic vibronic coupling (eq 15).

The $2A_g^-$-state Raman spectra of all the isotope species below 1600 cm^{-1} are not completely different from the $1A_g^-$-state Raman spectra, although the Raman lines have not been analyzed in detail. Most importantly, the strongest Raman lines at 1528, 1463, 1493, and 1451 cm^{-1} for [NA], [^{2}H], [^{13}C], and [^{2}H,^{13}C] β-carotenes, respectively, can be assigned to another a_g-type mode that is pushed down by strong vibronic coupling with the $3A_g^-$ state (vide infra). A detailed assignment of the rest of the Raman lines will be given only after normal-coordinate analysis, including the effect of vibronic coupling, has been performed.

Table 1 summarizes the ν_1 frequencies in the $2A_g^-$ and $1A_g^-$ states and their differences for [NA], [^{2}H], [^{13}C], and [^{2}H,^{13}C] β-carotenes. The ratio of the strengths of vibronic coupling

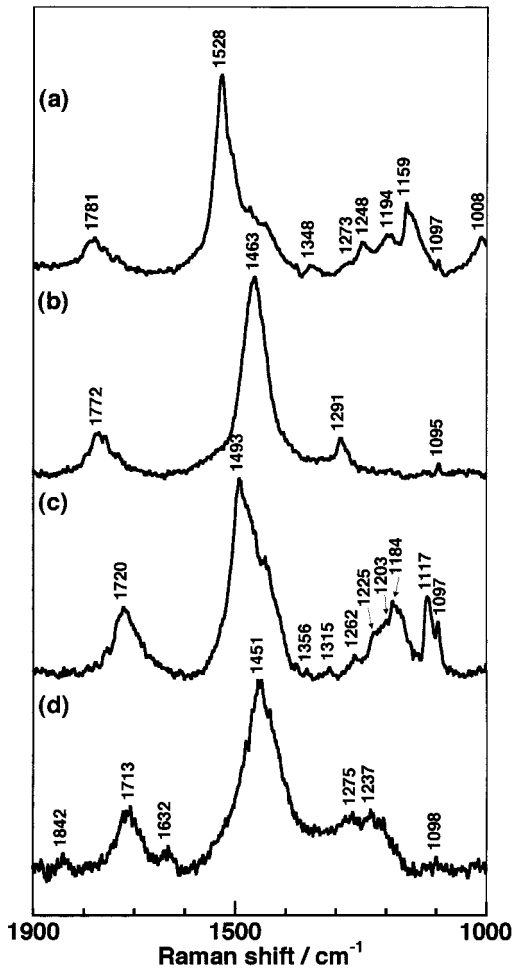

Figure 5. $2A_g^-$ (S_1)-state Raman spectra of (a) [NA], (b) [^{2}H], (c) [^{13}C], and (d) [^{2}H,^{13}C] *all-trans*-β-carotenes in THF solution (pumped and probed at 527 nm). A pair of Raman spectra were recorded with high and low power, and a difference spectrum was regarded as the $2A_g^-$-state Raman spectrum.

among the isotope species is now determined, by the use of the frequency differences as a measure, to be 1:1.21:0.89:1.07.

Estimation of the $2A_g^-$ to $1A_g^-$ Internal-Conversion Rate Using the Frequency Difference between the $2A_g^-$- and $1A_g^-$-State, ν_1 Modes as a Measure of the Vibronic-Coupling Strength. In the theoretical subsection of the Methods section, it was shown that the rate of internal conversion is given by

$$k = \frac{\pi}{\hbar} C^2 \frac{1}{\sqrt{2\pi(\Delta E)\hbar\omega}} \exp(-{}^1/_2\Delta^2) \exp\left(-\frac{\gamma(\Delta E)}{\hbar\omega}\right) \quad (9)$$

$$\gamma = \ln\frac{2(\Delta E)}{\Delta^2\hbar\omega} - 1 \quad (10)$$

when a single (ν_1) mode functions as both the promoting and the accepting mode. First, we regard the ν_1 frequency in the $1A_g^-$ state as that of the accepting mode, that is, $\hbar\omega = 1520$ cm^{-1}. Second, introduction of additional parameters, $\Delta E = 14\,600$ cm^{-1} (Sashima et al. unpublished) and $\Delta = 1.6$,[27] leads to a value of $\gamma = 1.02$. Thus, we regard γ to be unity. Third, we assume that the nonadiabatic vibronic-coupling constant (C) is proportional to the adiabatic vibronic-coupling constant (V), and we assume that the difference in the ν_1 frequency between the $2A_g^-$ and the $1A_g^-$ states is proportional to the adiabatic vibronic-coupling constant. Then, the relative rates of internal conversion can be obtained by a simplified equation,

$$\frac{k_I}{k_{NA}} = \frac{\Delta\nu_I}{\Delta\nu_{NA}} \exp\left[14\,600 \times \left(\frac{1}{\nu_{NA}} - \frac{1}{\nu_I}\right)\right] \quad (19)$$

Table 2 (second line) compares the relative rates of the $2A_g^-$ to $1A_g^-$ internal conversion thus estimated with those observed (from Table 1). The observed ratio of [NA] / [^{2}H] / [^{13}C] / [^{2}H,^{13}C] = 1.00:0.92:0.70:0.64 is now predicted to be 1.00:0.80:0.72:0.60. The agreement, except for [^{2}H], in which the ν_1 mode is drastically modified by the decoupling of the C=C stretching from the C−D in-plane bendings (vide supra), indicates that the ν_1 mode plays a major role in the internal conversion from the $2A_g^-$ to the $1A_g^-$ state.

Theoretical Calculations of the Isotopic Effects on the Strength of Vibronic Coupling and the Rate of Internal Conversion. *(i) The ν_1 Frequencies.* We first calculated, by Wilson's GF matrix method, the normal vibrations of the polyene model, docosaundecaene (hereafter simply called "polyene") and the β-carotene model ("β-carotene") having the methyl groups. In the calculations of polyene, we used both force constants that were listed in Table 3 and force constants that were partially transferred from a set determined for β-carotene by Saito and Tasumi.[28] In the calculations of β-carotene, we used the complete set of force constants determined by Saito and Tasumi.[28] Table 4 lists each pair of the ν_1 frequencies that were calculated with and without the off-diagonal carbon−carbon stretching force constants, including k(C=C·C=C), k(C−C·C−C), and k(C=C·C−C) (hereafter, we call them "the cross terms"): The results are compared with the observed values, that is, both an average of the ν_1 frequencies in the $1A_g^-$ and $2A_g^-$ states and the ν_1 frequency in the $1A_g^-$ state, which can be correlated with the diabatic and adiabatic frequencies, Ω and ω, respectively (see eqs 13 and 14). It is seen that the cross terms are useful to fit (push down) the ground ($1A_g^-$)-state ν_1 frequency. This is quite reasonable because we could show that the effect of the adiabatic vibronic-coupling constant is equivalent to that of introducing the non-Urey−Bradley, off-diagonal force constants (see the Appendix).

(ii) The L_x Matrixes. Figure 6 shows the displacements of the carbon and hydrogen atoms in the ν_1 mode (this is called "the L_x matrix") calculated for polyene (a) without and (b) with the cross terms and for β-carotene (c) without and (d) with the cross terms. The force constants of Saito and Tasumi[28] were used for both cases to facilitate comparison. It is clearly seen that the cross terms strongly affect the pattern of the ν_1 normal mode, although the change depends on how the cross terms were introduced empirically. More sophisticated ab initio calculations such as done for shorter polyenes[29] are necessary to precisely determine the cross terms.

The effects of the isotopic substitutions and of the molecular geometry on the ν_1 mode can be extracted from this set of figures: (i) The ^{2}H substitution (see [^{2}H] and [^{2}H,^{13}C] β-carotenes) almost completely removes the contributions of the methine in-plane bending and the methyl in-plane deformation vibrations, and it changes the pattern of the ν_1 normal mode to a large extent. On the other hand, the ^{13}C substitution affects the normal mode very little, although the displacements of the carbon atoms are slightly suppressed in comparison with those of the hydrogen atoms. (ii) The molecular structure drastically affects the type of normal mode that is involved. In polyene, the C−H in-plane bending and the C=C and C−C stretchings are coupled with each other to form a normal mode extending over the entire conjugated chain. In β-carotene, on the other

TABLE 2: The Observed, Estimated, and Calculated Relative Rates of the $2A_g^-$ to $1A_g^-$ Internal Conversion for [NA], [^{2}H], [^{13}C], and [^{2}H,^{13}C] *all-trans*-β-Carotenes

case	model	force field	cross terms	[NA]	[^{2}H]	[^{13}C]	[^{2}H,^{13}C]	average	standard deviation
	"observed"			1.00	0.92	0.70	0.64	0.81	0.18
	"estimated"[a]			1.00	0.80	0.72	0.60	0.78	0.17
(a)	polyene	Table 3	−	1.00	0.94	0.68	0.64	0.82	0.18
(c)		Saito and Tasumi[b]	−	1.00	0.95	0.70	0.64	0.82	0.18
(d)	β-carotene	Saito and Tasumi[b]	−	1.00	0.84	0.68	0.57	0.77	0.19

[a] On the basis of the relative strength of vibronic coupling, determined by $\Delta\nu$ as a measure (see Table 1). [b] See ref 28.

TABLE 3: Force Constants for the Polyene Model

stretching[a]		bending[b]		nonbonded repulsive[c]		cross terms[d]	
K(C=C)	6.500	H(C=C−C)	0.330	F(C=C−C)	0.350	k(C=C·C=C)	−0.350
K(C−C)	4.000	H(C=C−H)	0.224	F(C=C−H)	0.520	k(C−C·C−C)	−0.100
K(C−H)	4.830	H(C−C−H)	0.193	F(C−C−H)	0.490	k(C=C·C−C)	0.430
		H(H−C−H)	0.310				

[a,c,d] In mdyn·Å^{-1} and [b]in mdyn·Å.

TABLE 4. Observed and Calculated Frequencies of the ν_1 (In−Phase C=C Stretching) Mode

case	model	force field	cross terms	[NA]	[^{2}H]	[^{13}C]	[^{2}H,^{13}C]	average	standard deviation
	"observed"	$[\nu_1(1A_g^-) + \nu_1(2A_g^-)]/2$		1652	1615	1605	1574	1611	32
		$\nu_1(1A_g^-)$		1522	1458	1489	1435	1476	38
(a)	polyene	Table 3	−	1665	1631	1608	1570	1618	40
(b)			+	1525	1468	1481	1415	1472	46
(c)		Saito and Tasumi[a]	−	1687	1637	1634	1577	1634	45
(d)			+	1543	1449	1506	1398	1474	64
(e)	β-carotene	Saito and Tasumi[a]	−	1669	1626	1615	1565	1619	43
(f)			+	1524	1441	1487	1389	1460	58

[a] See ref 28.

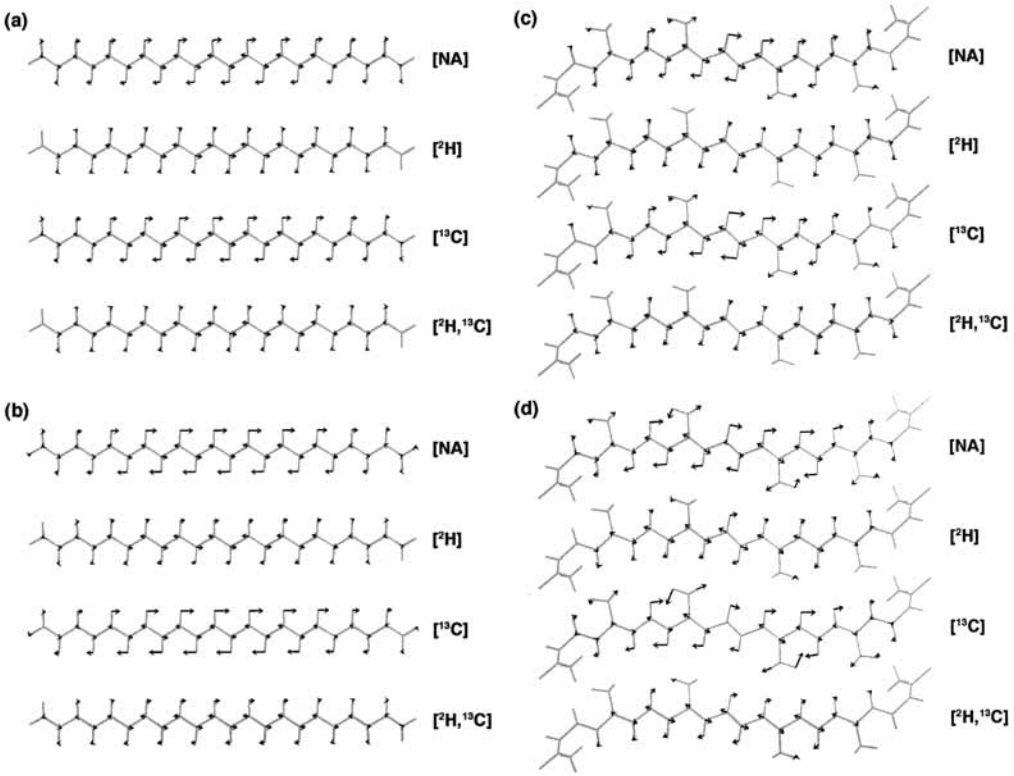

Figure 6. Displacements of the carbon and hydrogen atoms in the ν_1 mode calculated for isotopic polyenes (a) without and (b) with the carbon−carbon stretching cross terms and those calculated for isotopic β-carotenes (c) without and (d) with the cross terms, both using the set of force constants determined by Saito and Tasumi.[28]

hand, the methyl groups attached to the conjugated chain intervene the methine in-plane bendings, and their in-plane deformations couple with the preexisting C−H in-plane bending modes. For example, the central C=C and C−C stretchings, which are coupled with the methine in-plane deformations, are localized between the 13 and 13′ methyl groups. This situation gives rise to stronger isotopic effects (vide infra).

(iii) The L Matrixes. Now, we describe the L matrix that is necessary to calculate the adiabatic vibronic-coupling constant (equation 16): Because we are going to evaluate explicitly the

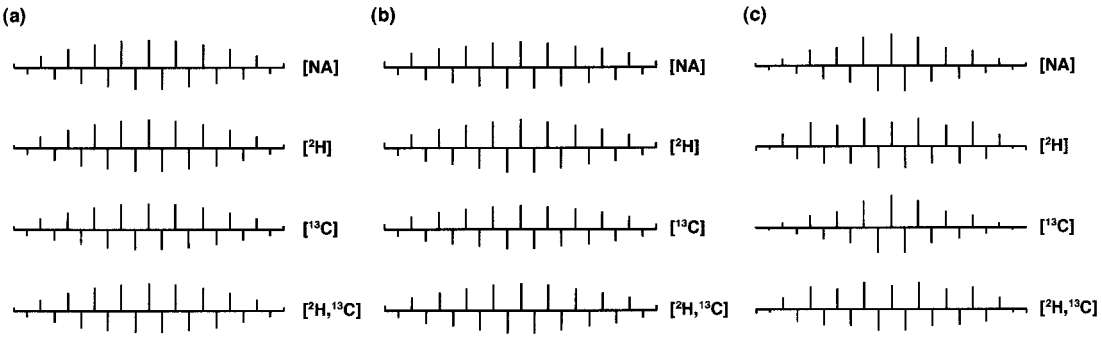

Figure 7. *L* matrixes of the ν_1 mode for isotopic polyenes calculated by removing the carbon−carbon stretching cross terms from (a) the set of force constants listed in Table 3, and (b) the force constants which were transferred from those determined for *all-trans*-β-carotene by Saito and Tasumi.[28] (c) *L* matrixes for isotopic β-carotenes were also calculated by removing the cross terms from the complete set of force constants determined for *all-trans*-β-carotene by Saito & Tasumi.[28] Bars above and below each horizontal line indicate the stretching and the shrinkage of the alternating C═C and C−C bonds; the C_{15}═$C_{15'}$ bond is at the center.

effect of vibronic coupling as the adiabatic vibroic-coupling constant, we use the results of normal-coordinate calculation *without* the cross terms. Figure 7 shows the *L* matrixes of isotopic polyenes calculated by using (a) the force constants in Table 3 and (b) those transferred from Saito and Tasumi.[28] The *L* matrixes were calculated for (c) β-carotene as well, by using the complete set (except for the cross terms) of force constants of Saito and Tasumi.[28] Here, the bars above and below each horizontal line indicate the stretching of the C═C bond and the shrinkage of the C−C bond for the alternating C═C and C−C bonds. In each calculation, the characteristic of the ν_1 mode is clearly seen, that is, the alternating C═C stretching and C−C shrinkage are all taking place in-phase with magnitudes decreasing systematically from the center to both ends. (When the transition bond-order matrix had a similar pattern in the $2A_g^-$ to $1A_g^-$ transition, strong vibronic coupling should take place (vide infra).) The isotopic effects are scattered all over the conjugated chain, and the effect of the force constants used are indistinguishable in polyene (compare Figure 7a to 7b). On the other hand, the presence of the methyl groups in β-carotene tends to localize the displacements in the central part (see above), and as a result, the isotope effects are clearly seen in the central C_{15}═$C_{15'}$ stretching, for example (Figure 7c).

(iv) The Transition Bond-Order Matrixes. We calculated the transition bond-order matrixes by the PPP−SD−CI method for a model polyene, docosaundecaene. Figure 8 shows the transition bond-order matrixes for transitions (a) between the $1A_g^-$ state and the $2A_g^-$, $1B_u^-$, $1B_u^+$, and $3A_g^-$ states, and (b) between the $2A_g^-$ state and the $1A_g^-$, $1B_u^-$, $1B_u^+$, and $3A_g^-$ states. The bars above and below each horizontal line indicate increase and decrease in transition bond order for the alternating double and single bonds, upon the relevant electronic transition. The bottom pair of the transition bond-order matrixes in Figure 6a and b, showing an increase in the C═C transition bond order and a decrease in the C−C transition bond order whose magnitude reduces systematically from the center to both ends, indicates that the $2A_g^-$ state and the $1A_g^-$ state can vibronically couple with each other when mediated by the ν_1 mode. This shows the corresponding pattern in the stretching of the C═C bond and the shrinkage of the C−C bond. In β-carotene, the presence of the methyl groups must substantially affect the electronic structure of the conjugated chain and, as a result, the transition bond-order matrixes. However, it is not straightforward to calculate the transition bond-order matrixes for the β-carotene skeleton or the contribution of σ-electrons.

(v) The Adiabatic Vibronic-Coupling Constants. We calculated the adiabatic vibronic constants by the use of the transition bond-order matrix that was calculated for polyene and the *L*

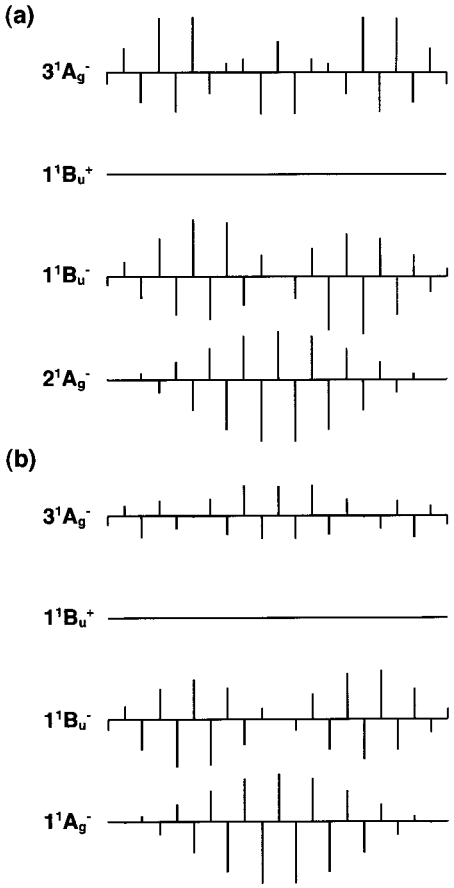

Figure 8. Transition bond-order matrixes (a) between the $1A_g^-$ state and the $2A_g^-$, $1B_u^-$, $1B_u^+$, and $3A_g^-$ states and (b) between the $2A_g^-$ state and the $1A_g^-$, $1B_u^-$, $1B_u^+$, and $3A_g^-$ states, which were calculated by the PPP−SD−CI method for a model polyene, docosaundecaene. Bars above and below each horizontal line indicate increase and decrease in transition bond order in the alternating double and single bonds located along the horizontal line (the C_{15}═$C_{15'}$ bond is in the center).

matrixes that were calculated (without the cross terms) for isotopic polyenes and β-carotenes (see eq 16). Table 5 compares the ratio of the calculated adiabatic vibronic-coupling constants (*V*) with that of the differences in the ν_1 frequency between the $2A_g^-$ and $1A_g^-$ states ($\Delta\nu$) (Table 1). In case (a), that is, when the *L* matrixes were calculated in polyene by the use of the force constants in Table 3, the relative strengths of vibronic coupling, as defined by the adiabatic vibronic-coupling constants, are in good agreement with the ones observed, as defined

TABLE 5. Observed and Calculated Relative Strengths of Vibronic Coupling for [NA], [^{2}H], [^{13}C] and [^{2}H,^{13}C] *all-trans*-β-Carotenes

case	model	force field	cross terms	[NA]	[^{2}H]	[^{13}C]	[^{2}H,^{13}C]	average	standard deviation
	"observed"			1.00	1.21	0.89	1.07	1.04	0.13
(a)	polyene	Table 3	−	1.00	1.13	0.93	1.08	1.04	0.09
(c)		Saito and Tasumi[a]	−	1.00	1.22	0.92	1.15	1.07	0.14
(e)	β-carotene	Saito and Tasumi[a]	−	1.00	1.06	0.91	1.02	1.00	0.06

[a] See ref 28.

by the differences in the ν_1 frequency; the value for [^{2}H] is an exception, which is underestimated. In case (c), that is, when the *L* matrixes were obtained by the use of the force constants of Saito and Tasumi,[28] the agreement in [^{2}H] is better, but the relative strength of [^{2}H,^{13}C] is overestimated. In case (e), that is, β-carotene, the relative strength in [^{2}H] is substantially underestimated. This may be due to either the effect of the *L* matrix reflecting the different type of ν_1 mode caused by deuteration or the usage of the transition bond-order matrix that was calculated for polyene (and not for β-carotene).

(vi) The Relative Rates of Internal Conversion. Finally, we calculated the relative rates of internal conversion (equation 9 with $\gamma = 1$) by regarding the adiabatic vibronic-coupling constant (*V*) as being proportional to the nonadiabatic vibronic-coupling constant (*C*). Table 2 compares the calculated relative rates of internal conversion with those "observed" and "estimated". In both case (a) and case (c) of polyene, the calculated relative rates are in excellent agreement with the observed rates, irrespective of the (diagonal) force constants used. The average values and the standard deviations are also in good agreement between the calculated and the observed rates. In case (d) of β-carotene, the relative rate for [^{2}H] is underestimated. It is interesting that the value is in better agreement with that estimated using the observed frequency difference ($\Delta\nu$) between the $2A_g^-$ and the $1A_g^-$ states. This result strongly suggests that the disagreement comes from the ν_1 vibrational mode, which is strongly affected by deuteration (vide supra). All of the above results prove that both (1) our method of analysis for the isotopic effects on the vibronic coupling and on the rate of internal conversion and (2) the notion that the in-phase, C═C stretching (ν_1) mode plays a dominant role in the $2A_g^- - to - 1A_g^-$ internal conversion process are correct.

Implication of the All-Trans Conjugated Chain and the C═C Stretching Vibrations within It for the Light-Harvesting and the Photoprotective Functions of Carotenoids in the Antenna Complexes. Natural selection of the carotenoid configurations has been found in purple bacteria and other photosynthetic organisms; the all-trans configuration is selected by the antenna complexes, whereas the 15-cis configuration is selected by the reaction centers.[1,30] The selection of the all-trans configuration is most probably due to the approximate C_{2h} symmetry of the extended conjugated chain that can generate the optically allowed $n^1B_u^+$ states and the optically forbidden $n^1A_g^-$ and $n^1B_u^-$ states. The basis for this conclusion will be described below.

Figure 8 characterizes the low-lying singlet levels of carotenoids in terms of transition bond-order matrixes. Figure 8a shows the transition bond-order matrixes between the $1A_g^-$ state and upper low-lying singlet excited states; Figure 8b shows the transition bond-order matrixes between the $2A_g^-$ state and low-lying singlet states, including both the ground and other excited states. Within the framework of the PPP approximation, the present theory predicts the following three pathways of internal conversion among the low-lying singlet states (see also Figure 1): (1) The $1B_u^-$ to $2A_g^-$ internal conversion that is facilitated by vibronic coupling through a b_u-type C═C stretching vibration, presumably having the pattern of C═C stretching and C−C shrinkage similar to the pattern of increase and decrease of the transition bond order in the $1B_u^-$ to $2A_g^-$ transition bond-order matrix (denoted as "$1^1B_u^-$" in Figure 8b); the latter exhibits increase in the C═C transition bond order and decrease in the C−C transition bond order of the b_u-type. The extremely fast $1B_u^+$ to $2A_g^-$ internal conversion can be facilitated (a) by the mixing of the $1B_u^+$ and $1B_u^-$ states having similar state energies[6] and (b) by this $1B_u^-$ to $2A_g^-$ vibronic coupling. (2) The $2A_g^-$ to $1A_g^-$ internal conversion that is facilitated by vibronic coupling through the ν_1 mode, the mechanism of which has been established in the present investigation. In this case, the pattern of the transition bond-order matrix ("$2^1A_g^-$" in Figure 8a and "$1^1A_g^-$" in Figure 8b) is in good agreement with that of the *L* matrix (Figure 7). (3) The $3A_g^-$ to $2A_g^-$ internal conversion that is facilitated by vibronic coupling through another a_g-type mode, presumably having the C═C stretching and C−C shrinkage pattern similar to that of the $2A_g^-$ to $3A_g^-$ transition bond-order matrix ("$3^1A_g^-$" in Figure 6b). The presence of this vibronic coupling is supported by the strong Raman line shown in Figure 5, which is shifted to as low as 1528 cm^{-1} in [NA] β-carotene, even in the $2A_g^-$ state (vide supra). The above three types of vibronic couplings, which use different normal modes, and the resultant three pathways of internal conversion are a unique feature of the all-trans conjugated chain having the approximate C_{2h} symmetry. The other unique feature is the presence of the "completely isolated" $1B_u^+$ state (see Figure 8a and b). Within the framework of the PPP approximation, no vibronic coupling is supposed to take place for this electronic state.

The above unique features of the low-lying singlet states, concerning vibronic coupling and internal conversion, originate not only from the C_{2h} symmetry of the all-trans conjugated chain but also from its length, which determines the ordering and location of the relevant singlet levels.[31] These features facilitate two pathways of singlet-energy transfer to BChl in the antenna complexes, as described in the Introduction: Upon absorption of a photon, the carotenoid molecule is excited to the optically allowed $1B_u^+$ state, and the singlet energy can be transferred to the Q_x state of BChl within its lifetime ($\sim 10^{-13}$ s), which is governed by its mixing with the close-by $1B_u^-$ state and the resultant $1B_u^-$ to $2A_g^-$ internal conversion. The vibronically isolated $1B_u^+$ state functions as a temporary singlet-energy reservoir. After the internal conversion to the $2A_g^-$ state, there is another channel of singlet-energy transfer to the Q_y state of BChl. The optically forbidden character of the $2A_g^-$ state facilitates a longer lifetime (10^{-11} s), and therefore, enables this state to function as a more durable singlet-energy reservoir. This lifetime is determined by the $2A_g^-$ to $^1A_g^-$ internal conversion, whose detailed mechanism has been established in the present investigation.

The above considerations lead us to the conclusion that the carotenoid molecule in the all-trans configuration is well-designed both for harvesting and for transferring the singlet energy to BChl and for dissipating the excess singlet energy via the internal conversion processes. The all-trans carotenoids

seem to play a most important function of photoprotection in the antenna complexes, in addition to the well-recognized light-harvesting function. The extremely efficient, singlet-energy transfer reactions, which can compete with the extremely fast internal conversion processes, can be facilitated only by close contacts between the carotenoid and the BChl molecules, the detailed mechanisms of which have not been fully understood.[16,32,33]

Conclusions

The major role of the in-phase, C=C stretching (ν_1) mode in the $2A_g^-$ to $1A_g^-$ vibronic coupling and internal conversion has been shown by the use of isotopic effects on the strength of vibronic coupling and on the rate of internal conversion. The relative rates of internal conversion among isotope-labeled β-carotenes have been correctly predicted by a combination of (a) a theory expressing the adiabatic vibronic-coupling constant as a product of the transition bond-order matrix and the *L* matrix and (b) the Englman−Jortner equation containing the nonadiabatic coupling constant.[12]

The all-trans configuration of a carotenoid having approximate C_{2h} symmetry gives rise to unique excited-state properties including the vibronically isolated $1B_u^+$ state as well as the $2A_g^-$ to $1A_g^-$, $1B_u^-$ to $2A_g^-$ and $3A_g^-$ to $2A_g^-$ internal conversion processes. They facilitate two channels of singlet-energy transfer pathways to BChl (i.e., $1B_u^+ \rightarrow Q_x$ and $2A_g^- \rightarrow Q_y$) as well as at least three efficient relaxation pathways to dissipate the excess singlet energy. This is most probably the reason that the all-trans configuration has been selected by the carotenoids in the antenna complexes.

Acknowledgment. This work has been supported by a grant from the Science Research Promotion Fund.

Appendix

In this appendix, we try to show that the effect of the adiabatic vibronic-coupling constant is equivalent to that of the non-Urey−Bradley, off-diagonal stretching force constants. We denote the internal coordinates as R_i (which includes changes in bond lengths), bond angles, and torsional angles. It can be shown that the force constants of the *n*th adiabatic electronic state can be expressed as

$$F_{ij}^{(n)} = \left(\frac{\partial^2 V_\sigma(R)}{\partial R_i \partial R_j}\right)_{R=R^0} + \langle\bar{\psi}_n(R)|\sum_{r\neq s,\sigma} h_{rs,ij} a_{r\sigma}^\dagger a_{s\sigma}|\bar{\psi}_n(R)\rangle_{R=R^0} + 2\sum_{m\neq n}[\langle\bar{\psi}_n(R)| \sum_{r\neq s,\sigma} h_{rs,i} a_{r\sigma}^\dagger a_{s\sigma}|\bar{\psi}_m(R)\rangle\langle\bar{\psi}_m(R)|\sum_{r\neq s,\sigma} h_{rs,j} a_{r\sigma}^\dagger a_{s\sigma}|\bar{\psi}_n(R)\rangle]_{R=R^0}}{E_n(R^0) - E_m(R^0)} \quad \text{(i)}$$

with

$$h_{rs,ij} = \frac{\partial^2 \beta_{rs}}{\partial R_i \partial R_j} - {}^1/_2 P_{rs} \frac{\partial^2 \gamma_{rs}}{\partial R_i \partial R_j} \quad \text{(ii)}$$

and

$$h_{rs,i} = \frac{\partial \beta_{rs}}{\partial R_i} - {}^1/_2 P_{rs} \frac{\partial \gamma_{rs}}{\partial R_i} \quad \text{(iii)}$$

where V_σ is the energy of the σ system, R represents a set of $\{R_i\}$, and R^0 corresponds to the equilibrium geometry in the *n*th electronic state. The first two terms on the right-hand side of eq i is called the diabatic force constants. Because $\partial^2 V_\sigma(R)/\partial R_i \partial R_j \approx 0$, $\partial^2 \beta_{rs}/\partial R_i \partial R_j \approx 0$, and $\partial^2 \gamma_{rs}/\partial R_i \partial R_j \approx 0$ when R_i and R_j ($i \neq j$) represent changes in bond lengths, it is clear that the non-Urey−Bradley, off-diagonal terms of the adiabatic stretching-force constants mainly originate from the third term of eq i. The third term is related to $V_j^{(n,m)}$ by the following equation:

$$V_j^{(n,m)} \cong 2\sqrt{\frac{\hbar}{\omega_j^{(m)}}} \sum_{r\neq s} \langle\bar{\psi}_n(R)|\sum_\sigma h_{rs,rs} a_{r\sigma}^\dagger a_{s\sigma}|\bar{\psi}_m(R)\rangle_{R=R^0} \times L_{rs,j} \quad \text{(iv)}$$

where $h_{rs,rs} = \partial\beta_{rs}/\partial R_{rs} - 0.5 \times P_{rs} \times \partial\gamma_{rs}/\partial R_{rs}$. From this relation, it follows that the adiabatic vibronic-coupling constant, $V_j^{(n,m)}$, will vanish if the non-Urey−Bradley, off-diagonal terms of the adiabatic force constants become zero. This leads to the required statement.

References and Notes

(1) Koyama, Y.; Fujii, R. Cis−Trans Carotenoids in Photosynthesis: Configurations, Excited-State Properties and Physiological Functions. In *The Photochemistry of Carotenoids: Applications in Biology*; Frank, H. A., Cogdell, R. J., Young, A. J., Britton, G., Eds.; Kluwer Academic Publishers: Boston, p 161.

(2) Frank, H. A.; Cogdell, R. J. The Photochemistry and Function of Carotenoids in Photosynthesis. In *Carotenoids in Photosynthesis*; Young, A., Britton, G., Eds.; Chapman & Hall: London, 1993; p 252.

(3) Frank, H. A.; Cogdell, R. J. *Photochem. Photobiol.* **1996**, *63*, 257.

(4) Koyama, Y.; Kuki, M.; Andersson, P. O.; Gillbro, T. *Photochem. Photobiol.* **1996**, *63*, 243.

(5) Ricci, M.; Bradforth, S. E.; Jimenez, R.; Fleming, G. R. *Chem. Phys. Lett.* **1996**, *259*, 381.

(6) Sashima, T.; Nagae, H.; Kuki, M.; Koyama, Y. *Chem. Phys. Lett.* **1999**, *299*, 187.

(7) Kuki, M.; Hashimoto, H.; Koyama, Y. *Chem. Phys. Lett.* **1990**, *165*, 417.

(8) Fujii, R.; Onaka, K.; Kuki, M.; Koyama, Y.; Watanabe, Y. *Chem. Phys. Lett.* **1998**, *288*, 847.

(9) Hashimoto, H.; Koyama, Y. *Chem. Phys. Lett.* **1989**, *154*, 321.

(10) Noguchi, T.; Kolaczkowski, S.; Arbour, C.; Aramaki, S.; Atkinson, G. H.; Hayashi, H.; Tasumi, M. *Photochem. Photobiol.* **1989**, *50*, 603.

(11) Wasielewski, M. R.; Johnson, D. G.; Bradford, E. G.; Kispert, L. D. *J. Chem. Phys.* **1989**, *91*, 6691.

(12) Englman, R.; Jortner, J. *Mol. Phys.* **1970**, *18*, 145.

(13) Lin, S. H. *J. Chem. Phys.* **1966**, *44*, 3759.

(14) O'Malley, T. F. Diabatic States of Molecule −Quasistationary Electronic States. In *Advances in Atomic and Molecular Physics*; Bates, D. R., Esterman, I., Eds.; Academic Press: New York, 1971; Vol. 7; p 223.

(15) Negri, F.; Orlandi, G.; Zerbetto, F.; Zgierski, M. Z. *J. Chem. Phys.* **1989**, *91*, 6215.

(16) Nagae, H.; Kakitani, T.; Katoh, T.; Mimuro, M. *J. Chem. Phys.* **1993**, *98*, 8012.

(17) Donath, W. E. *J. Chem. Phys.* **1964**, *41*, 626.

(18) Kuki, M.; Nagae, H.; Cogdell, R. J.; Shimada, K.; Koyama, Y. *Photochem. Photobiol.* **1994**, *59*, 116.

(19) Sterling, C. *Acta Crystallogr.* **1964**, *B26*, 214.

(20) Shimanouchi, T. *Computer Programs for Normal Coordinate Treatment of Polyatomic Molecules*; University of Tokyo: Tokyo, 1968.

(21) Harris, E. H. *The Chlamydomonas Sourcebook*; Academic Press: San Diego, 1989.

(22) Sashima, T.; Abe, M.; Kurano, N.; Miyachi, S.; Koyama, Y. *J. Phys. Chem.* **1998**, *102*, 6903.

(23) Omata, T.; Murata, N. *Plant Cell Physiol.* **1983**, *24*, 1093.

(24) Tsukida, K.; Saiki, K.; Takii, T.; Koyama, Y. *J. Chromatogr.* **1982**, *245*, 359.

(25) Koyama, Y.; Hosomi, M.; Miyata, A.; Hashimoto, H.; Reames, S. A.; Nagayama, K.; Kato-Jippo, T.; Shimamura, T. *J. Chromatogr.* **1988**, *439*, 417.

(26) Limantara, L.; Fujii, R.; Zhang, J.-P.; Kakuno, T.; Hara, H.; Kawamori, A.; Yagura, T.; Cogdell, R. J.; Koyama, Y. *Biochemistry* **1998**, *37*, 17469.

(27) Onaka, K.; Fujii, R.; Nagae, H.; Kuki, M.; Koyama, Y.; Watanabe, Y. *Chem. Phys. Lett.* in press.

(28) Saito, S.; Tasumi, M. *J. Raman Spectrosc.* **1983**, *14*, 310.

(29) Hirata, S.; Torii, H.; Tasumi, M. *J. Chem. Phys.* **1995**, *103*, 8964.

(30) (a) Koyama, Y.; Mukai, Y. Excited States of Retinoids, Carotenoids and Chlorophylls As Revealed by Time-Resolved, Electronic Absorption and Resonance Raman Spectroscopy. In *Biomolecular Spectroscopy Part B*; Clark, R. J. H., Hester, R. E., Eds.; John Wiley & Sons: Chichester, 1993; Vol. 21, p 49. (b) Koyama, Y. *J. Photochem. Photobiol.* **1991**, *B9*, 265.

(31) Tavan, P.; Schulten, K. *J. Chem. Phys.* **1986**, *85*, 6602.

(32) Scholes, G. D.; Harcourt, R. D.; Fleming, G. R. *J. Chem. Phys.* **1997**, *B101*, 7302.

(33) Damjanovic, A.; Ritz, T.; Schulten, K. *Phys. Rev.* **1999**, *E59*, 3293.

(34) Sashima, T.; Shiba, M.; Hashimoto, H.; Nagae, H.; Koyama, Y. *Chem. Phys. Lett.* **1998**, *290*, 36.